Topology Optimization for Orthotropic Supports in Additive Manufacturing

Matías Godoy

Topology Optimization for Orthotropic Supports in Additive Manufacturing

Matías Godoy[1]

[1]CMAP, CNRS, Ecole Polytechnique, Institut Polytechnique de Paris, 91128 Palaiseau, France. matias.godoy@cmap.polytechnique.fr

1 Introduction

In this report, we investigate a problem that arises within the scope of support structures in additive manufacturing. Support structures are employed in Additive Manufacturing (AM) to guarantee the quality of the final product. They are utilized, for instance, to handle overhanging regions where the final product is not self-supporting, or to prevent deformations in the final product due to thermal residual stresses.

In the study [1], various mathematical models are introduced to address these issues, leading to optimization problems that are numerically solved using the level set topology optimization method [2]. In this framework, the support structure is assumed to be composed of an *isotropic* material, that is, a material with uniform mechanical properties in all directions.

In our research, we address the challenge of printing a shape ω along with its supports S, aiming to minimize the *compliance*. The material of the shape ω is considered isotropic, whereas the material of the supports S is deemed *orthotropic*, a material with distinct mechanical properties in mutually orthogonal directions. This assumption might be realistic as, in actual manufacturing, the supports are grid structures, which could be modelled as an equivalent volume possessing different material properties in each direction. Following [1], we focus on the case where the compliance minimization occurs while assuming the shape ω to be fixed; in other words, we aim to identify the supports for the structure ω that are influenced only by their own weight. We examine a two-dimensional reference case to explore potential qualitative differences when stronger material properties are imposed in certain directions, comparing these results with the isotropic case.

This study is motivated as a component of the research project SOFIA (**SO**lutions pour la **F**abrication **I**ndustrielle **A**dditive metallique), which is primarily aimed at contributing to new developments in AM technologies.

2 Anisotropic Supports

Anisotropic materials are characterized by their differing material properties when we examine their mechanical properties in relation to different directions. A subset of these materials are orthotropic materials, which have material properties that differ along mutually-orthogonal axes of rotational symmetry. In contrast, isotropic materials possess the same properties regardless of the direction of measurement.

We begin by exploring the formulations involved and the main changes compared to the isotropic setting.

Given a shape ω and the supports S, both being open sets of $\mathbb{R}^d$ ($d = 2$ or $d = 3$), with ω composed of an isotropic material and S composed of an *orthotropic* material, we note that the shape ω in this study is fixed, and only the supports S are optimized. The supported structure, denoted as $\Omega = S \cup \omega$, is, as usual, assumed to be contained within a rectangular *build chamber* D. The baseplate will always represent the bottom boundary of D, and is denoted as $\Gamma_D := \{x \in D : x_d = 0\}$. Unless otherwise stated, we assume the support is clamped to the baseplate Γ_D. The remaining regions of the boundary of the supported structure Ω are traction-free, denoted by Γ_N. In the following, we consider the space, for $\Omega \subset \mathbb{R}^d$ an open set, and Γ a $(d-1)$-dimensional set:

$$H^1_\Gamma(\Omega)^d := \left\{ u \in H^1(\Omega)^d : \ u = 0 \text{ on } \Gamma \right\} \tag{2.1}$$

The supported structure Ω is governed by linearized elasticity, with only gravity forces being applied to Ω. In this context, optimizing the support S to minimize the compliance of Ω will result in minimal overhang regions. The elastic displacement u_{spt} of the supported structure $\Omega = \omega \cup S$ is the unique solution in the space $H^1_{\Gamma_D}(\Omega)$ to the mechanical system:

$$\begin{cases} -\operatorname{div}(\sigma(u_{spt})) = \rho g & \text{in } \Omega, \\ u_{spt} = 0 & \text{on } \Gamma_D, \\ \sigma(u_{spt}) n = 0 & \text{on } \Gamma_N. \end{cases} \tag{2.2}$$

Here, σ is the *stress tensor*, which is related to the *strain tensor* e. In the linearized case, this is given by $e(u) = \frac{1}{2}\left(\nabla u + \nabla u^T\right)$, via Hooke's law:

$$\sigma = Ce, \tag{2.3}$$

where C is a fourth order tensor, often referred to as the *elasticity tensor* or simply as the 'Hooke's law' of the material. Using the minor and major symmetries of the tensor C, due to the symmetry of the tensors σ and e, we can rewrite the relation in a vector form, using Voigt notation (see [5]), as:

$$\sigma = Ae. \tag{2.4}$$

Now, A is a matrix and σ, e are vectors using Voigt notation. The explicit form of C (or A) will depend on the considered material properties and, in our specific case, will be of particular interest. As we are considering materials with different properties in each 'part' (shape or supports), this will, in particular, imply that we will consider (analogously for C):

$$A_\Omega = A_\omega \chi_\omega + A_S \chi_S,$$

where $\chi_{\mathcal{O}}$ is the indicator function for the set $\mathcal{O}$. This decomposition indicates that the mechanical properties of the fixed shape ω and the optimizable supports S will, in general, be assumed to be different, with a *sharp-interface*.

When the considered material is *isotropic*, we can relate the quantities $\sigma(u)$ with $e(u)$ in the form:

$$\sigma(u) = Ce(u) = 2\mu e(u) + \lambda \operatorname{tr}(e(u)) \operatorname{Id} = 2\mu e(u) + \lambda \operatorname{div} u \operatorname{Id} \tag{2.5}$$

where μ, λ are the Lamé coefficients of the material. This will be the setting for the fixed part ω.

Remark 2.1. *The variational formulation for the system* (2.2) *in the isotropic case is:*

$$\begin{cases} \text{Find } u \in H^1_{\Gamma_D}(\Omega) \text{ such that, for any } v \in H^1_{\Gamma_D}(\Omega): \\ \displaystyle\int_\Omega 2\mu e(u) \cdot e(v)\ dx + \int_\Omega \lambda \mathrm{div}\, u \mathrm{div}\, v\ dx = \int_\Omega \rho g \cdot v\ dx \end{cases} \tag{2.6}$$

however, in anisotropic cases, we cannot expect to have such a compact formula.

How do things change when the material is anisotropic? Let us focus on the orthotropic case, in which we have, in Voigt notation:

$$\begin{bmatrix} \sigma_1 \\ \sigma_2 \\ \sigma_3 \\ \sigma_4 \\ \sigma_5 \\ \sigma_6 \end{bmatrix} = \begin{bmatrix} C_{11} & C_{12} & C_{13} & 0 & 0 & 0 \\ C_{12} & C_{22} & C_{23} & 0 & 0 & 0 \\ C_{13} & C_{23} & C_{33} & 0 & 0 & 0 \\ 0 & 0 & 0 & C_{44} & 0 & 0 \\ 0 & 0 & 0 & 0 & C_{55} & 0 \\ 0 & 0 & 0 & 0 & 0 & C_{66} \end{bmatrix} \begin{bmatrix} e_1 \\ e_2 \\ e_3 \\ e_4 \\ e_5 \\ e_6 \end{bmatrix} \tag{2.7}$$

This implies, in the most general case, that the derivatives of u (and the test function v) are weighted differently compared to the compact formula (2.5). We will specify these quantities in the next section.

The mechanical performance of the structure Ω is measured by means of its structural compliance, given by:

$$J(S) = \int_{\omega \cup S} Ae(u_{spt}) \cdot e(u_{spt}) dx = \int_{\omega \cup S} \rho g \cdot u_{spt} dx\ . \tag{2.8}$$

The latter equality comes from the variational formulation of the problem taking the test function as the solution u_{spt}. It is worth noting that, therefore, this quantity is (explicitly) independent of the Hooke's law considered (however, it is implicitly dependent on it, as u_{spt} depends on it). The admissible supports for this problem are allowed in the following set:

$$\mathcal{U}_{ad} := \{S \subset (D \setminus \omega) \text{ such that, } \Gamma_D \cap \partial S \neq \emptyset,\ \partial\omega \cap \partial S \neq \emptyset\} \tag{2.9}$$

And also notice that the objective functional, in order to avoid trivial solutions, will be

$$\mathcal{L}(S) := J(S) + \ell\ Vol(S) \tag{2.10}$$

where ℓ is a Lagrange multiplier (a penalization parameter or adjusted parameter in the optimization process).

In order to minimize (2.10) with respect to the admissible supports $\mathcal{U}_{ad}$, we rely on the concept of shape derivatives, based on the Hadamard boundary variation method (see [6]), this is: we measure the changes on the cost given by (2.10) whenever the set S is perturbed by a vector field $\theta \in W^{1,\infty}(\mathbb{R}^d, \mathbb{R}^d)$ in the sense:

$$\theta \mapsto S_\theta := (Id + \theta)(S),$$

with this, we can define the concept of shape derivative of a functional:

Definition 2.2. *A function $F : \mathcal{U}_{ad} \to \mathbb{R}$ is shape differentiable at S if the map $\theta \mapsto F(S_\theta)$ is Fréchet-differentiable at 0. The shape derivative, denoted $F'(S)$, satisfies the following asymptotic expansion:*

$$F(S_\theta) = F(S) + F'(S)(\theta) + o(\theta)$$

in a neighborhood of $0 \in W^{1,\infty}$.

Regardless of the Hooke's law considered, we have the following result (which can be obtained using, for example, the formal method of Céa; see [1, 4]):

Proposition 2.3. *Assuming $\theta \cdot n = 0$ on $\partial S \cap \partial\omega$ (this is, assuming that interface between ω and S is fixed). The shape derivative of the compliance (2.8) is given by*

$$J'(S)(\theta) = \int_{\partial S \cap \omega^c} (-Ae(u_{spt}) \cdot e(u_{spt}) + 2\rho g \cdot u_{spt})\ \theta \cdot n\ ds \tag{2.11}$$

where u_{spt} is the solution of (2.2) and the compliment of ω is with respect to D, and $\partial S \cap \omega^c = \partial S \setminus \partial\omega$.

Remark 2.4. *It is important to note that this formula is valid only under the assumption that the shape ω remains fixed (which is a realistic assumption in the case when, for design reasons, we cannot change it). If we allow optimizing ω and S simultaneously, the different material properties between ω and S will impose additional terms to the shape derivative and the hypothesis $\theta \cdot n = 0$ on the interface will no longer be valid. See [1] for details for such a problem.*

Remark 2.5. *Thanks to the previous proposition, we can find a descent direction θ for the cost functional $\mathcal{L}$, which is given by:*

$$\theta = -(-Ae(u_{spt}) \cdot u_{spt} + 2\rho g \cdot u_{spt} + \ell)n = -vn, \tag{2.12}$$

with this, we obtain:

$$\mathcal{L}'(S)(\theta) = \int_{\partial S \cap \omega^c} -v^2 ds < 0$$

which, using the asymptotic expansion from definition 2.2, allows us, for a small enough t, to obtain a shape $S_{t\theta}$ with a smaller cost: $\mathcal{L}(S_{t\theta}) < \mathcal{L}(S)$.

2.1 Orthotropic Material: 2D Case

When we consider a 2-dimensional scenario, we are saying that the case under study is a *plane strain* problem, that is, a problem where the displacement takes place only in two orthogonal directions. This is equivalent to the following definition.

Definition 2.6. *If the strain state at a material particle is such that the only non-zero strain components act in one plane only, the particle is said to be in plane strain.*

Choosing the plane XY as the plane where the strains are non-zero, we have

$$e_{xz} = e_{yz} = e_{zz} = 0 \tag{2.13}$$

So, the strain matrix becomes

$$e = \begin{bmatrix} e_{xx} & e_{xy} & 0 \\ e_{xy} & e_{yy} & 0 \\ 0 & 0 & 0 \end{bmatrix} \tag{2.14}$$

and, in this case, Hooke's law becomes, in Voigt notation:

$$\begin{bmatrix} \sigma_{11} \\ \sigma_{22} \\ \sigma_{12} \end{bmatrix} = \begin{bmatrix} 2\mu_1 + \lambda & \lambda & 0 \\ \lambda & 2\mu_2 + \lambda & 0 \\ 0 & 0 & \gamma \end{bmatrix} \begin{bmatrix} e_{11} \\ e_{22} \\ 2e_{12} \end{bmatrix} \tag{2.15}$$

In principle, λ should also differ in each direction; however, for the sake of simplicity, we will keep it constant as it will be sufficient for testing purposes to consider different Young's modulus. The variational formulation of (2.2), assuming that the entire material in Ω is orthotropic, becomes:

$$\begin{cases} \text{Find } u \in H^1_{\Gamma_D}(\Omega) \text{ such that, for all } v \in H^1_{\Gamma_D}(\Omega): \\ \int_\Omega 2\mu_1 \partial_1 u_1 \partial_1 v_1 + \lambda(\partial_1 u_1 + \partial_2 u_2)(\partial_1 v_1 + \partial_2 v_2)\ dx \\ + \int_\Omega 2\mu_2 \partial_2 u_2 \partial_2 v_2 + \gamma(\partial_2 u_1 + \partial_1 u_2)(\partial_1 v_2 + \partial_2 v_1)\ dx \\ = \int_\Omega \rho g \cdot v\ dx \end{cases} \tag{2.16}$$

For our computations, we consider, instead of Lamé coefficients λ, μ, the Young's modulus E_i and the Poisson ratio ν (this latter one fixed to 0.3). The coefficients are related in the following way (in the isotropic case)

$$\mu = \frac{E}{2(1+\nu)}, \lambda = \frac{E\nu}{(1+\nu)(1-2\nu)}$$

in our simplified case we will consider:

$$\mu_i = \frac{E_i}{2(1+\nu)},\ \lambda = \frac{E_\omega \nu}{(1+\nu)(1-2\nu)},$$

where E_ω stands for the Young's modulus of the fixed part ω, and E_1 and E_2 will be the Young's modulus in the horizontal ($i = 1$) and vertical ($i = 2$) directions for the support S. This will be (roughly) a measure of the strength of the support S in each direction.

2.2 The Level-Set Method for Shape Optimization

The level-set method, proposed by Osher and Sethian (see [10]) for tracking fronts and free boundaries, is used for various applications in image processing and fluid mechanics, among others. In structural optimization, it has been suggested as a powerful tool by Allaire, Jouve, and Toader (see [2]), which allows for shape and topological optimization in this context with reduced computational cost, avoiding unnecessary remeshing.

In this context, consider a computational working domain $D \subset \mathbb{R}^d$ in which all admissible shapes S are included, such that the loaded boundaries Γ_D, Γ_N are included in ∂D. The mesh on D is fixed, and the shape S of the actual support is implicitly defined by a level set function ϕ, defined on D, as follows:

$$\begin{cases} \phi(x) < 0 \Leftrightarrow x \in S \\ \phi(x) = 0 \Leftarrow x \in \partial S \cap D \\ \phi(x) > 0 \Leftrightarrow x \in D \setminus S \end{cases}$$

We are interested in computing the shape derivative $J'(S)(\theta)$ given by (2.11), and we need to compute the solution of the system (2.2). However, since Ω is implicitly defined by the level set function, no mesh is available to solve it. To overcome this issue, we employ the *Ersatz approach*. This involves filling the complementary part $D \setminus (S \cup \omega)$ with an extremely soft material, characterized by Hooke's tensor εA with $\varepsilon \ll 1$ (typically $\varepsilon = 10^{-3}$), and then we solve the problem defined on the entire computational domain D:

$$\begin{cases} -\text{div}\,(A_\varepsilon e(u_{spt})) = \rho g & \text{in } D, \\ u_{spt} = 0 & \text{on } \Gamma_D, \\ \sigma(u_{spt}) n = 0 & \text{on } \Gamma_N, \end{cases} \tag{2.17}$$

with $A_\varepsilon(x) := \begin{cases} A = A_\omega \chi_\omega + A_S \chi_S & \text{if } x \in \Omega \ \varepsilon A_\omega \\ \text{if } x \in D \setminus \Omega. \end{cases}$

This method is proven to be consistent (see [3]).

To track the evolution of the shape S as we perform the minimization of the cost functional $\mathcal{L}$, we must relate the movement of the level-set function ϕ for S^{k-1} (the shape of the supports at the $(k-1)$ iteration of the numerical algorithm) and the normal velocity $\theta = -vn$ given by (2.12). This ensures that the new shape $S^k := S^{k-1}_{t\theta}$ is such that $\mathcal{L}(S^k) < \mathcal{L}(S^{k-1})$. So, to transport the level set function ϕ along the gradient flow $\theta = -vn$, we solve the following linear transport equation (introducing a time variable for the step t):

$$\partial_t \phi + \theta \cdot \nabla \phi = 0 \text{ on } [0, \tau] \times D$$

which, for the given θ, provides the Hamilton-Jacobi equation:

$$\partial_t \phi - v \|\nabla \phi\| = 0 \text{ on } [0, \tau] \times D \tag{2.18}$$

with initial condition $\phi(0, x)$ taken as the input level set (without time). The new level set will correspond to $\phi(\tau, x)$.

Finally, it is important to note that to solve equation (2.18), we need a field θ defined on the entire box D, instead of the expression (2.12) deduced from the shape derivative (2.11), which is defined only on $\partial S \cap \omega^c$. To this end, following [7], we perform a process called *extension-regularization* of the velocity, solving the problem:

$$\begin{cases} \text{Find } Q \in H^1(\mathbb{R}^d) \text{ such that:} \\ \displaystyle\int_D \alpha_{reg}^2 \nabla Q \cdot \nabla v + Q \cdot v \ dx = \mathcal{L}'(\Gamma)(vn) \ \forall v \in H^1(\mathbb{R}^d) \end{cases} \tag{2.19}$$

where the parameter α_{reg} is the minimal element size from the mesh of D.

We can summarize the procedure in the following algorithm:

Algorithm 1 Shape Optimization of an Orthotropic Support Structure for a Fixed Part Minimizing the Compliance

Require: S^0, a given support structure and its level set function ϕ_0; ω, the fixed part.
  while $k \leq k_{maxiter}$ **do**
    Solve elasticity system on $\Omega^k = S^k \cup \omega$.
    Compute the normal velocity (descent direction) v^k using formula (2.12) and solving the extension-regularization problem (2.19).
    Set $t = initial_step$.
    while $j \leq j_{max}$ (Loop for Line search) **do**
      Let $\phi_j^k := \phi^k$.
      Transport ϕ^k solving (2.18) with $\theta = -v^k n$ using $\tau = t$.
      Compute Hooke's tensor A^k associated with the transported ϕ^k.
      if $\mathcal{L}(\Omega_{t\theta}^k) < (1 + tol)\mathcal{L}(\Omega^{k-1})$ **then**
        $\phi^k \leftarrow Transport(\phi^k)$
        break
      else
        $\phi^k \leftarrow \phi_j^k$ (Undo the transport).
        $t \leftarrow \max(0.5t, t_{min})$
      end if
      $j \leftarrow j + 1$
    end while
    New shape is defined by $x \in D : \ \phi^k(x) < 0$.
    Update parameters (augmented Lagrangian case)
    $k \leftarrow k + 1$
  end while

2.3 Numerical Testing

In the following, we consider a few tests in order to study how much a solution changes when the horizontal-vertical properties (the Young modulus E_i) change in orthotropic cases compared to the isotropic case: $E_1 = E_2$. We present two different geometries with several initialization procedures, recalling that, in general, we obtain local minima. For simplicity, in all the simulations, we take $\nu = 0.3$, $\gamma = \dfrac{\mu_1 + \mu_2}{2}$ and then we will test how the structure behaves when the Young modulus of the supports changes (this is, we only modify E_1, E_2 or, equivalently, μ_1, μ_2; where the index 1 is related to horizontal strength and 2 is related to vertical strength).

All the simulations are performed using the Finite Element software *FreeFEM++* (see [8]), and the transport of the level set is performed using the package *Advect* [9].

2.3.1 The Diagonal Shape

In this case, the geometry of the fixed part to be supported is a diagonal bar, with homogeneous Dirichlet boundary conditions at the bottom and right side of the domain $D = [0, 1] \times [0, 1]$, and the rest have homogeneous Neumann boundary conditions.

We consider two level set initializations, both of which are essentially the domain D covered by the support material with holes distributed with different symmetries:

- Case 1:

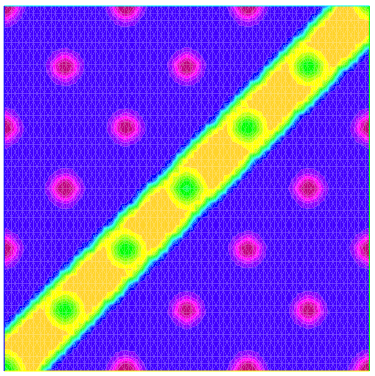

Figure 1: Initial level set function

For this configuration, we obtain the following final distribution of supports and convergence curves (volume and cost functional):

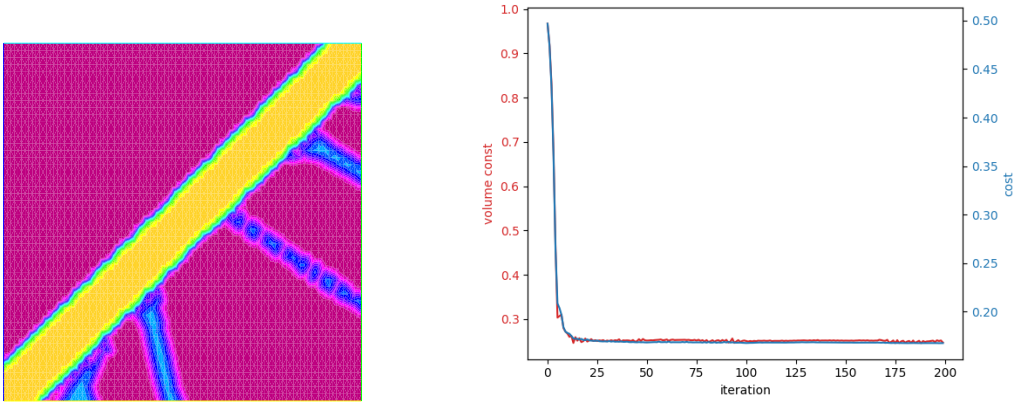

Figure 2: Anisotropic case: $E_1 = 1.0, E_2 = 0.1$

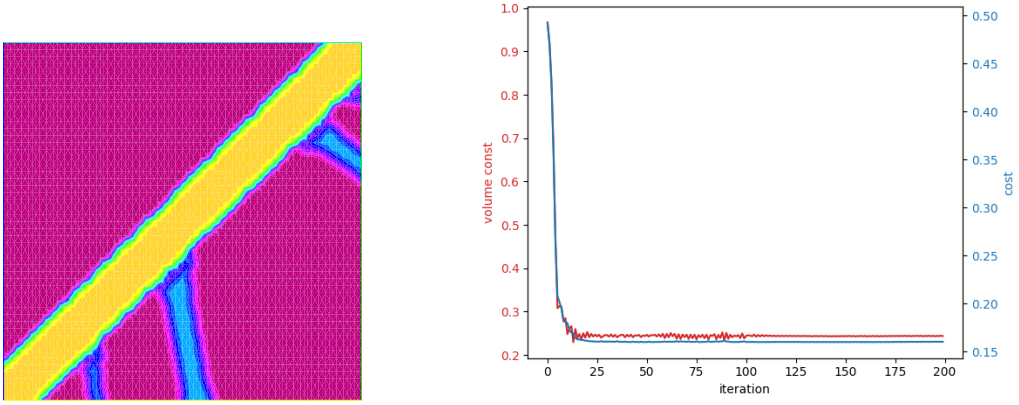

Figure 3: Anisotropic case: $E_1 = 0.1, E_2 = 1.0$

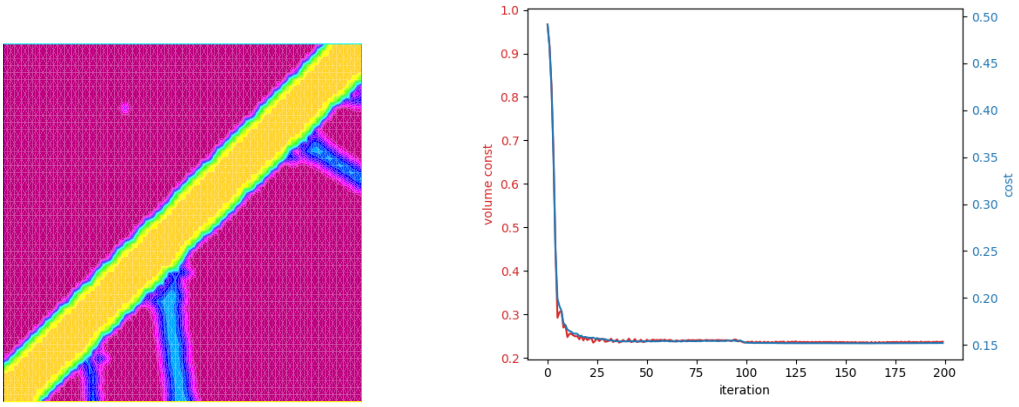

Figure 4: Isotropic case: $E_1 = E_2 = 1.0$

- Case 2:

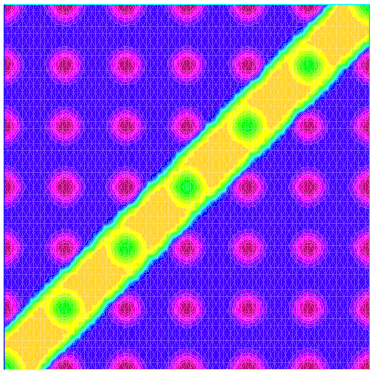

Figure 5: Initial level set function

For this configuration, we obtain the following final distribution of supports and convergence curves (volume and cost functional):

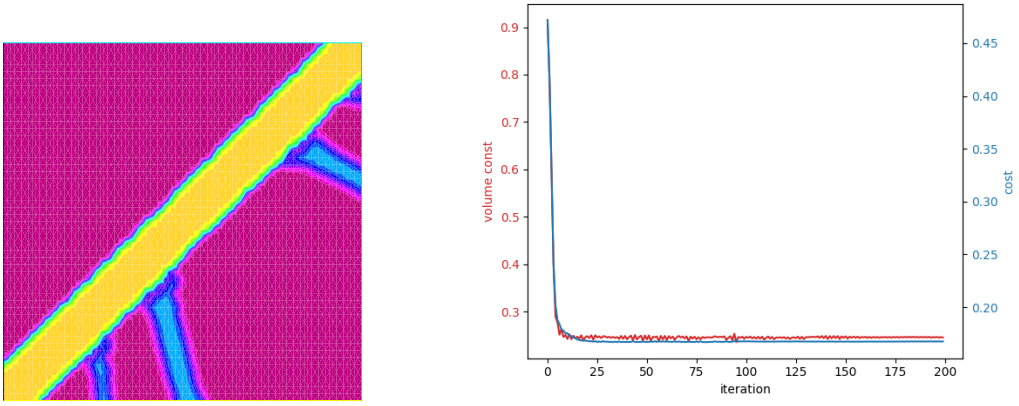

Figure 6: Anisotropic case: $E_1 = 1.0, E_2 = 0.1$

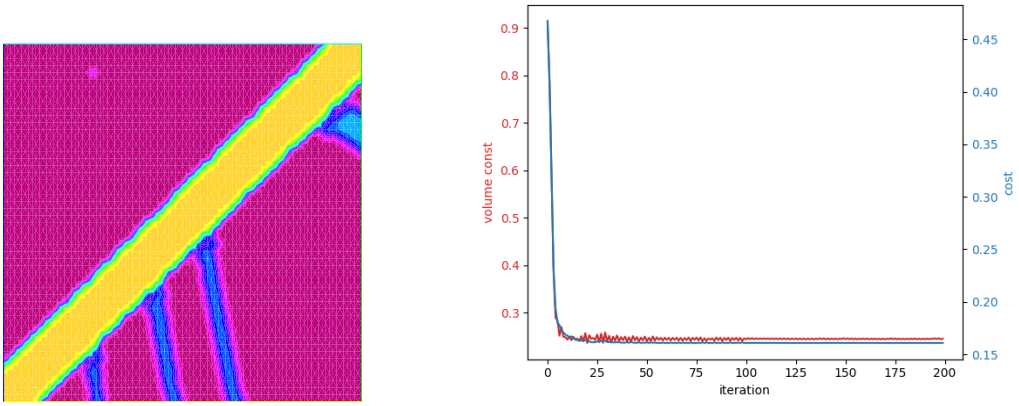

Figure 7: Anisotropic case: $E_1 = 0.1, E_2 = 1.0$

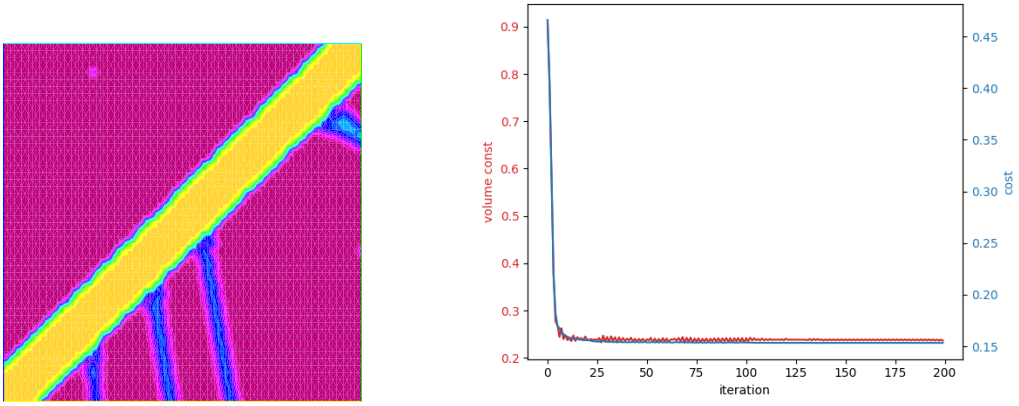

Figure 8: Isotropic case: $E_1 = E_2 = 1.0$

2.3.2 The L Shape

In this case, the geometry of the fixed part to be supported is an L shape with homogeneous Dirichlet boundary condition at the bottom of the domain $D = [0, 1] \times [0, 1]$, and the rest of the boundary has homogeneous Neumann boundary conditions.

- Case 1:

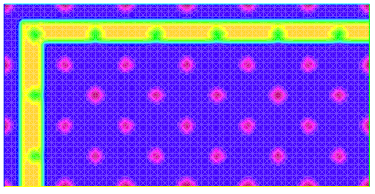

Figure 9: Initial level set function

For this configuration, we obtain the following final distribution of supports and convergence curves (volume and cost functional):

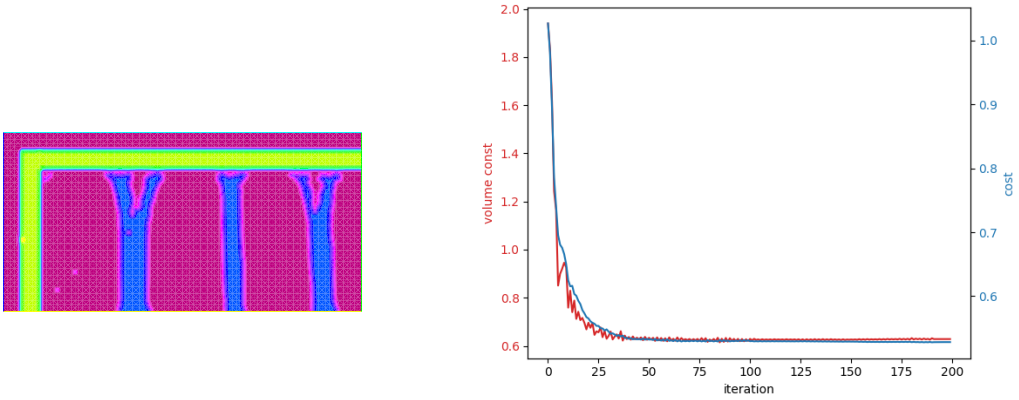

Figure 10: Anisotropic case: $E_1 = 1.0, E_2 = 0.1$

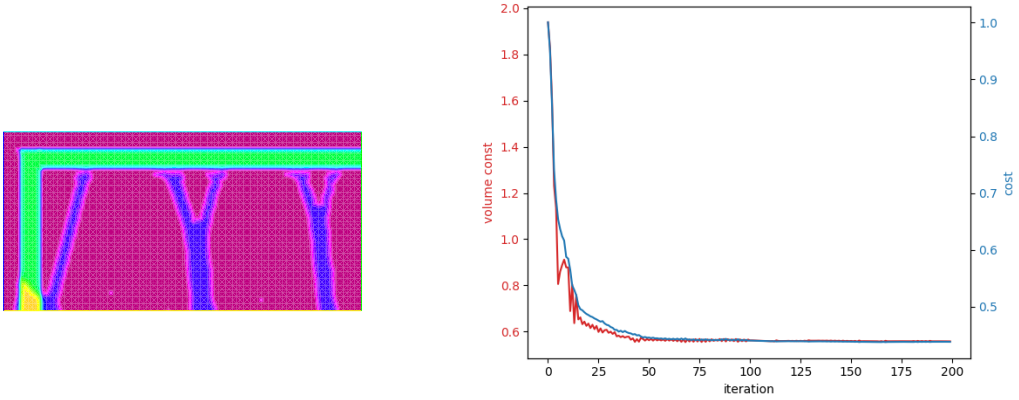

Figure 11: Anisotropic case: $E_1 = 0.1, E_2 = 1.0$

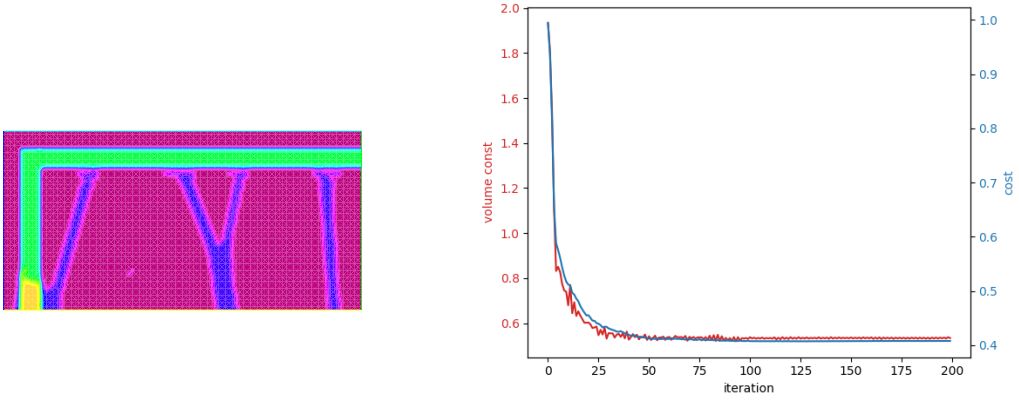

Figure 12: Isotropic case: $E_1 = E_2 = 1.0$

- Case 2:

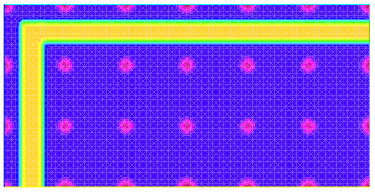

Figure 13: Initial level set function

For this configuration, we obtain the following final distribution of supports and convergence curves (volume and cost functional):

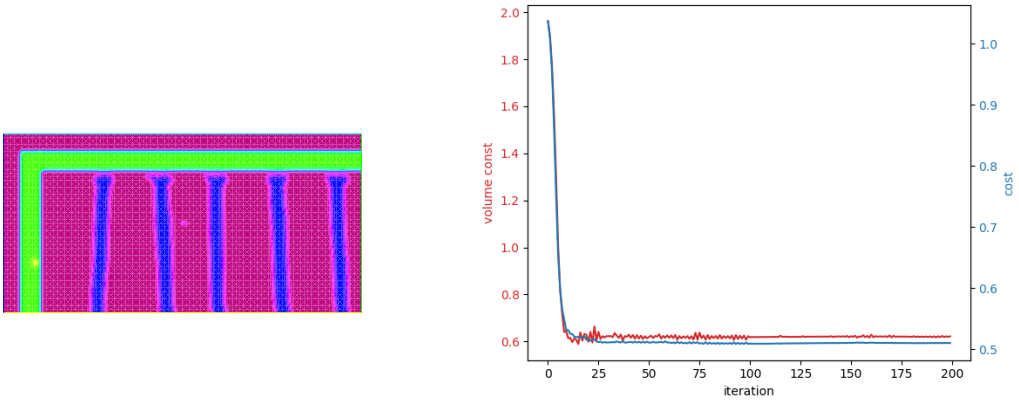

Figure 14: Anisotropic case: $E_1 = 1.0, E_2 = 0.1$

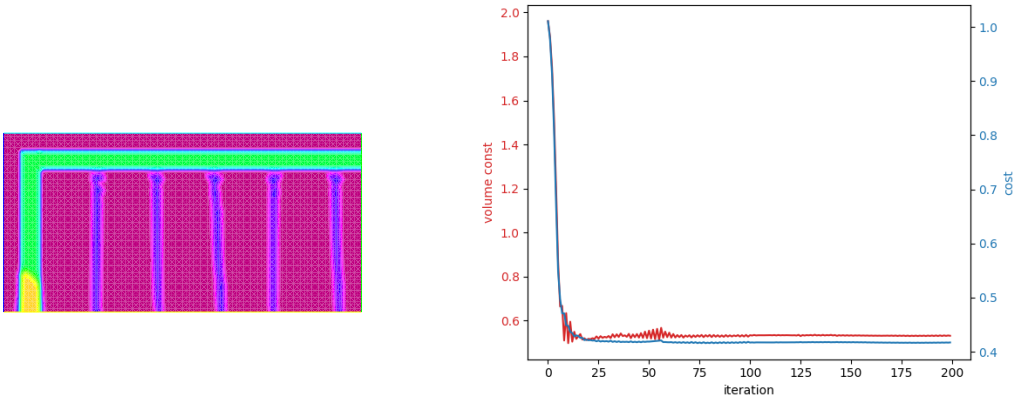

Figure 15: Anisotropic case: $E_1 = 0.1, E_2 = 1.0$

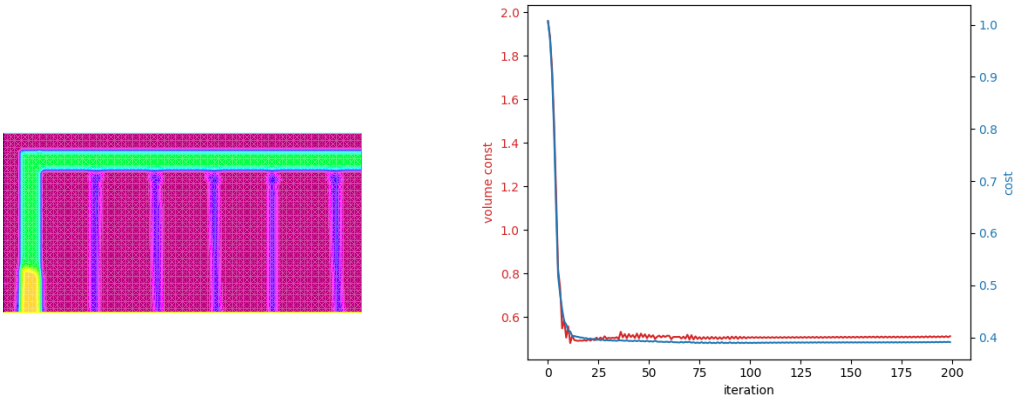

Figure 16: Isotropic case: $E_1 = E_2 = 1.0$

In this first series of examples, we observe some common behavior:

- The lowest value of the cost functional is reached in the isotropic case.
- Qualitatively, isotropic and 'vertically stronger' ($E_2 > E_1$) cases have similar topology. The 'horizontally stronger' case obtains the highest cost and its topology is different.
- As we mentioned before, the optimal shape could be different if the initialization is different, as we see in the L shape case.
- The reinforced zones tend to be similar in all cases, even when qualitatively the shapes for the supports are different.

2.3.3 The Diagonal Shape: Augmented Lagrangian

Next, we test the diagonal shape using an Augmented Lagrangian method for optimization. This allows us to impose a fixed objective volume for the supports, considering the following *merit* function to be optimized:

$$\mathcal{L}(\Omega, \lambda, \mu) := J(\Omega) - \lambda(Vol(\Omega) - V_{obj}) + \frac{\mu}{2}(Vol(\Omega) - V_{obj})^2$$

where V_{obj} is the objective volume and the coefficient λ is expected to converge to the Lagrange multiplier of the restriction $V = V_{obj}$. In order to do this, the theory (see [11]), suggests updating λ_{k+1} as:

$$\lambda_{k+1} = \lambda_k - \mu_k(Vol(\Omega) - V_{obj}),$$

It is important to note that in this case, it is not necessary to take a sequence of μ_k such that $\mu_k \to +\infty$. In our examples, we begin with $\mu = 0.1$ and update every 3 iterations as $\mu \leftarrow 1.3\mu$ while $\mu \leq \mu_{max} = 10.0$. We take in these examples:

$$\lambda_0 = -0.2, \;\; \lambda_0 = -\frac{1}{|\partial S \cap \omega^c|}\int_{\partial S \cap \omega^c} Ae(u) : e(u)\; ds; \;\; \mu_0 = \frac{|\lambda_0|}{2}.$$

We use the same configuration as before, imposing that the volume of the supports should be 10% of the volume of the shape in the first 3 cases, then 30% in the following 3 cases, and finally 50% in the last 3 cases.

- Case 1:

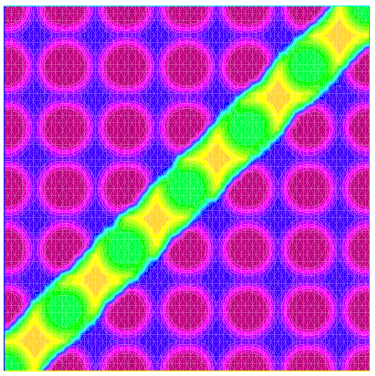

Figure 17: Initial level set function

For this configuration, we obtain the following final distribution of supports and convergence curves (volume and cost functional):

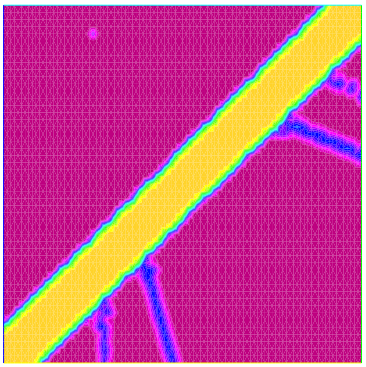

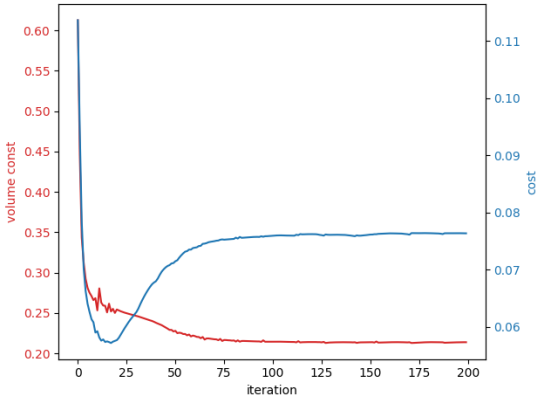

Figure 18: Anisotropic case: $E_1 = 1.0, E_2 = 0.1$

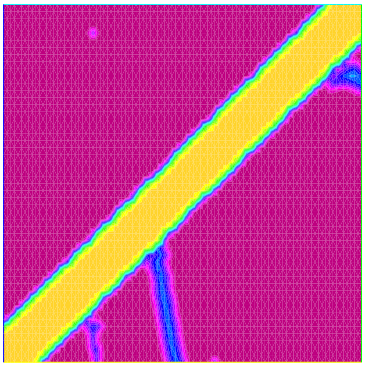

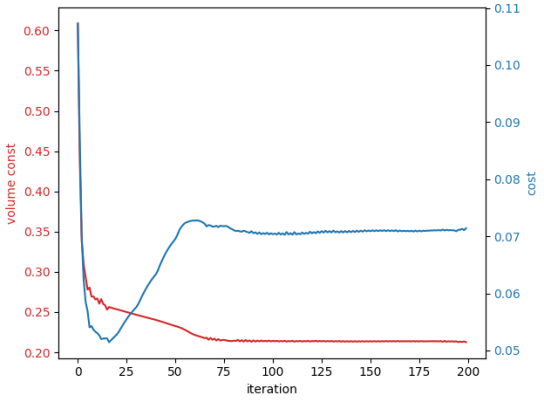

Figure 19: Anisotropic case: $E_1 = 0.1, E_2 = 1.0$

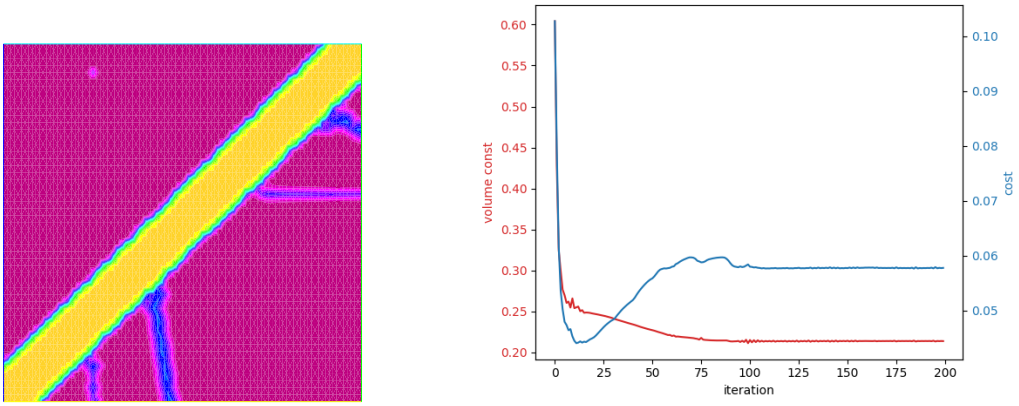

Figure 20: Isotropic case: $E_1 = E_2 = 1.0$

- Case 2:

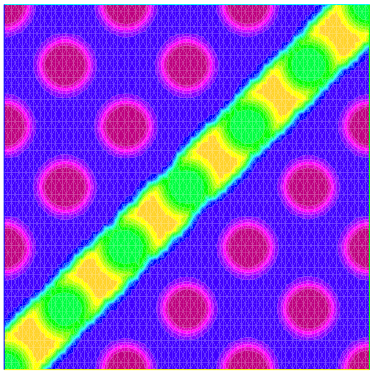

Figure 21: Initial level set function

For this configuration, we obtain the following final distribution of supports and convergence curves (volume and cost functional):

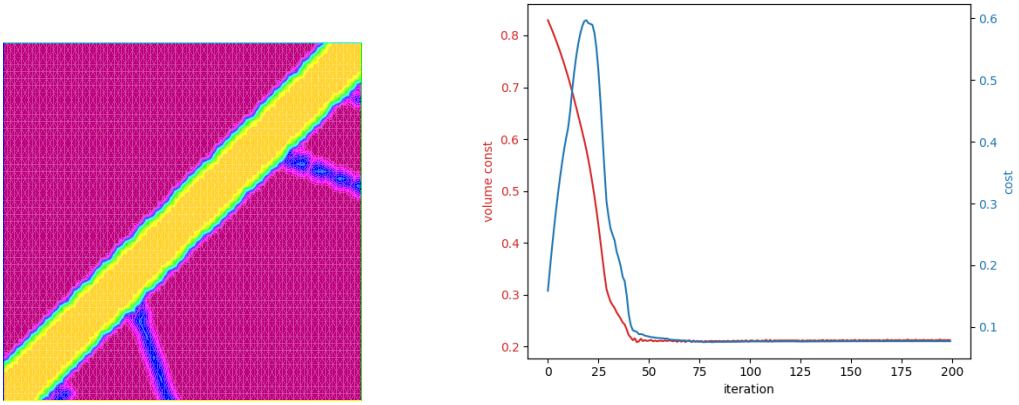

Figure 22: Anisotropic case: $E_1 = 1.0, E_2 = 0.1$

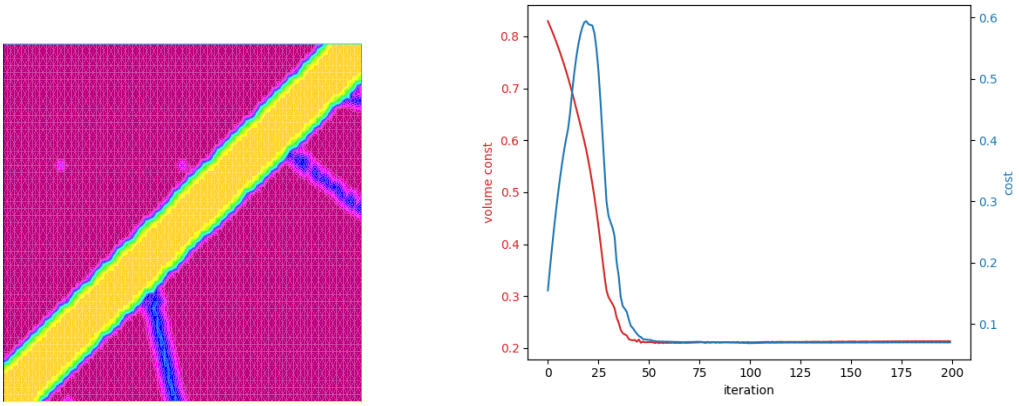

Figure 23: Anisotropic case: $E_1 = 0.1, E_2 = 1.0$

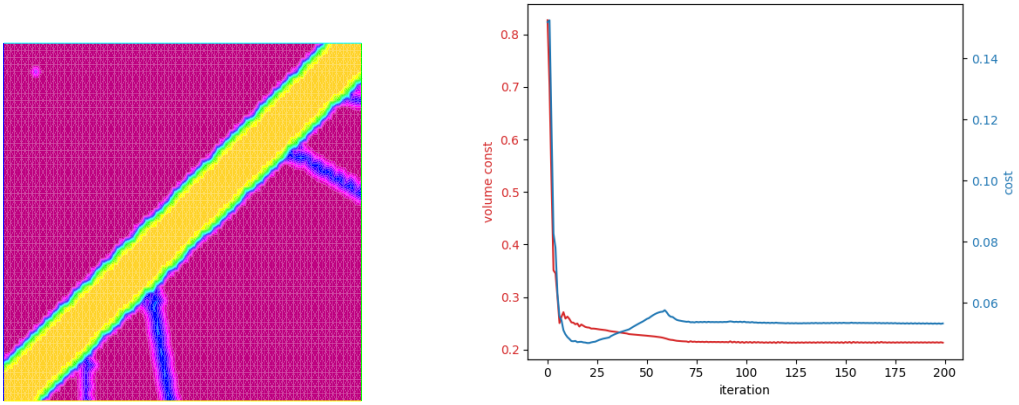

Figure 24: Isotropic case: $E_1 = E_2 = 1.0$

- Case 3:

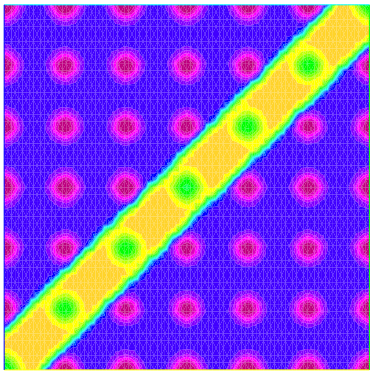

Figure 25: Initial level set function

For this configuration, we obtain the following final distribution of supports and convergence curves (volume and cost functional):

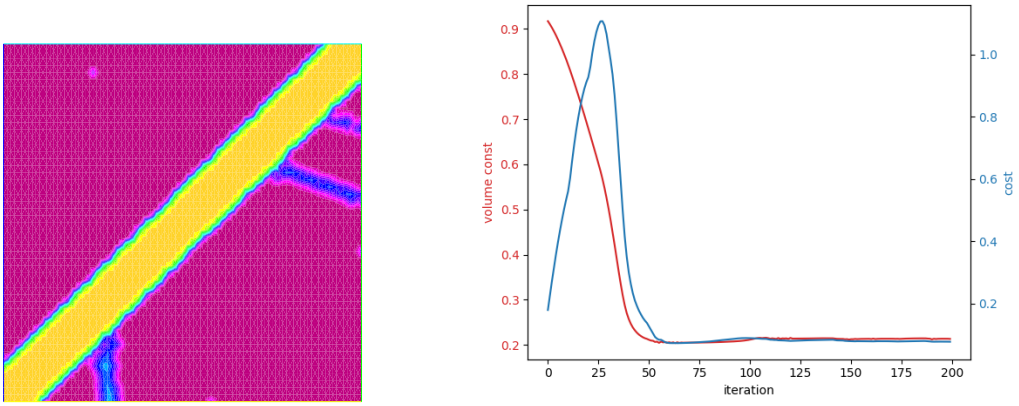

Figure 26: Anisotropic case: $E_1 = 1.0, E_2 = 0.1$

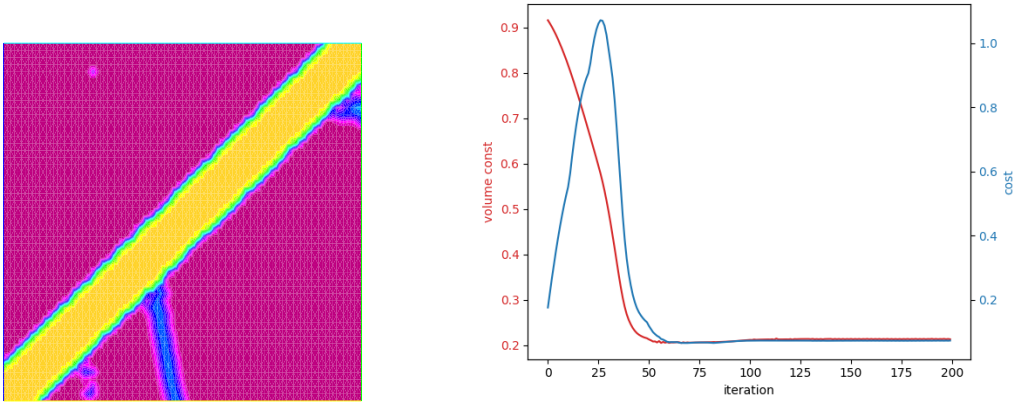

Figure 27: Anisotropic case: $E_1 = 0.1, E_2 = 1.0$

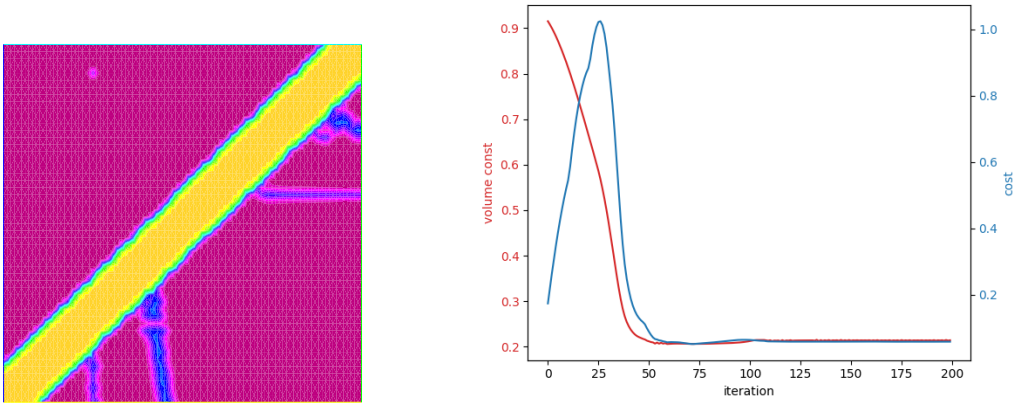

Figure 28: Isotropic case: $E_1 = E_2 = 1.0$

Remark: in the following three cases we have $V_{obj} = 1.3 \cdot V_{fixed}$.

- Case 4:

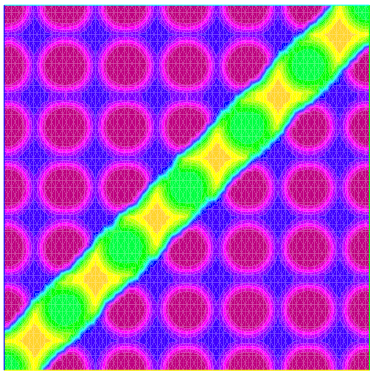

Figure 29: Initial level set function

For this configuration, we obtain the following final distribution of supports and convergence curves (volume and cost functional):

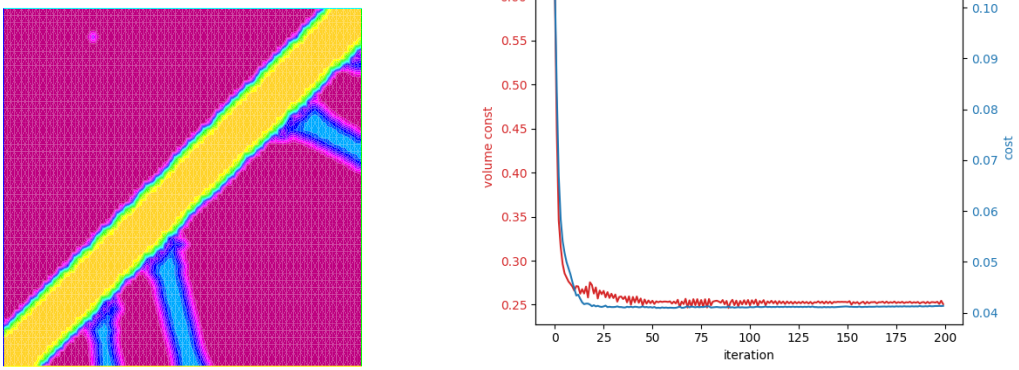

Figure 30: Anisotropic case: $E_1 = 1.0, E_2 = 0.1$

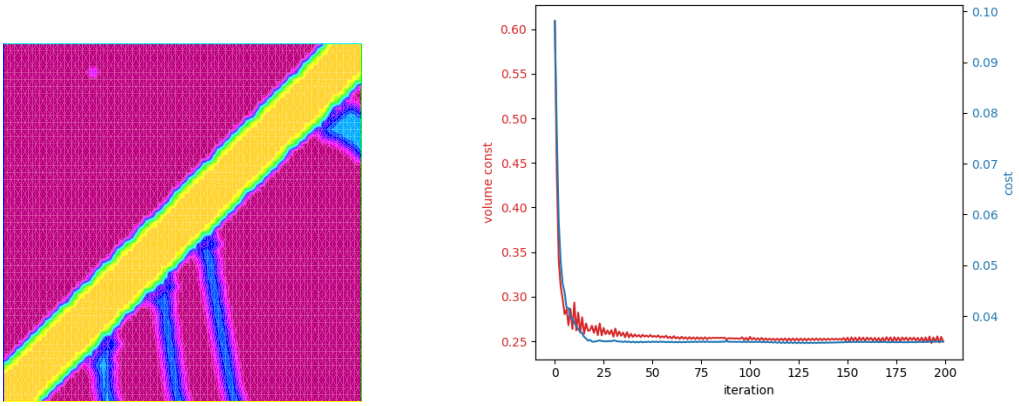

Figure 31: Anisotropic case: $E_1 = 0.1, E_2 = 1.0$

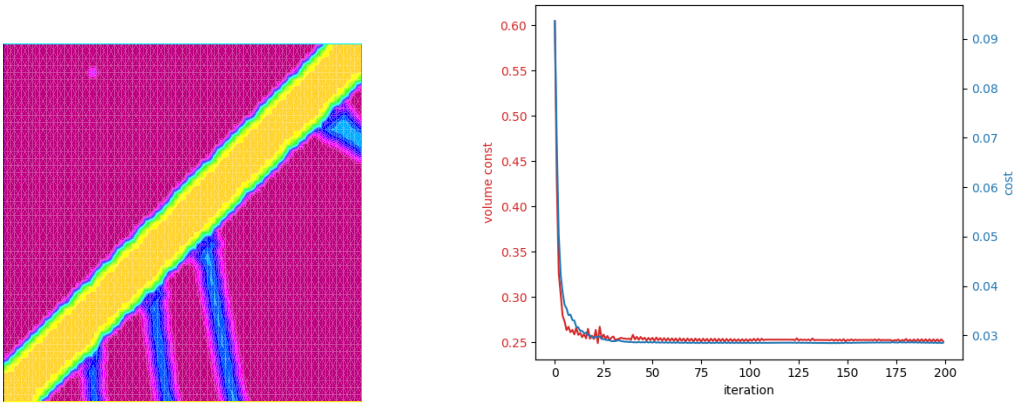

Figure 32: Isotropic case: $E_1 = E_2 = 1.0$

- Case 5:

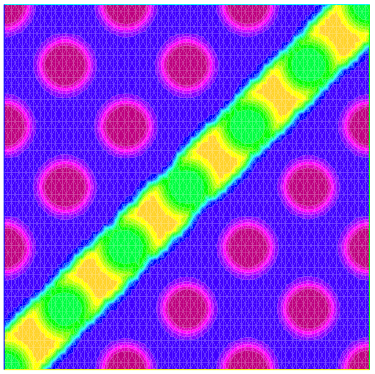

Figure 33: Initial level set function

For this configuration, we obtain the following final distribution of supports and convergence curves (volume and cost functional):

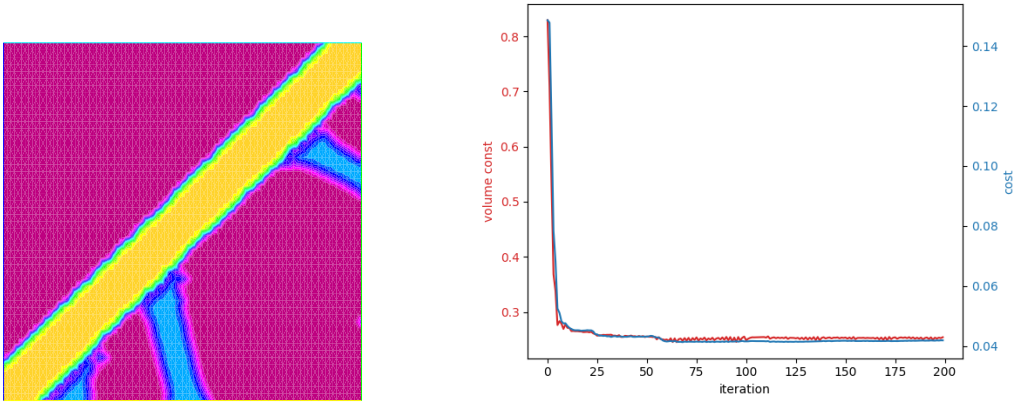

Figure 34: Anisotropic case: $E_1 = 1.0, E_2 = 0.1$

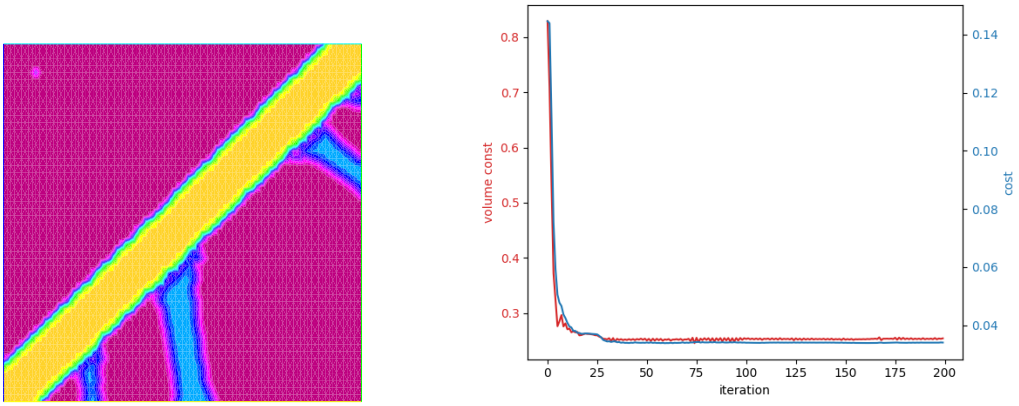

Figure 35: Anisotropic case: $E_1 = 0.1, E_2 = 1.0$

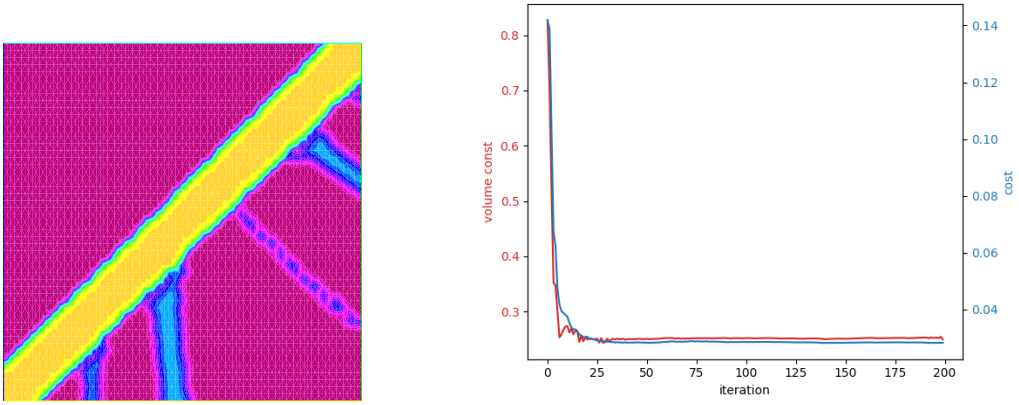

Figure 36: Isotropic case: $E_1 = E_2 = 1.0$

- Case 6:

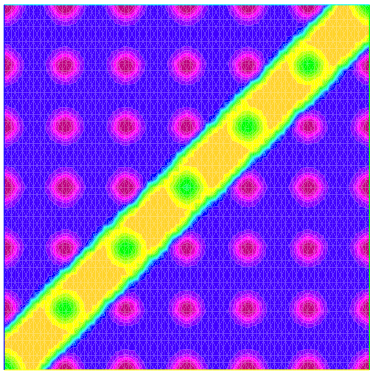

Figure 37: Initial level set function

For this configuration, we obtain the following final distribution of supports and convergence curves (volume and cost functional):

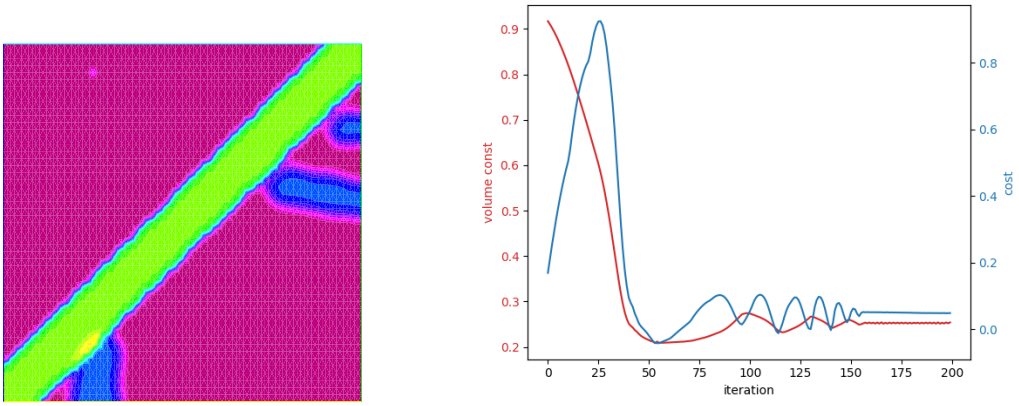

Figure 38: Anisotropic case: $E_1 = 1.0, E_2 = 0.1$

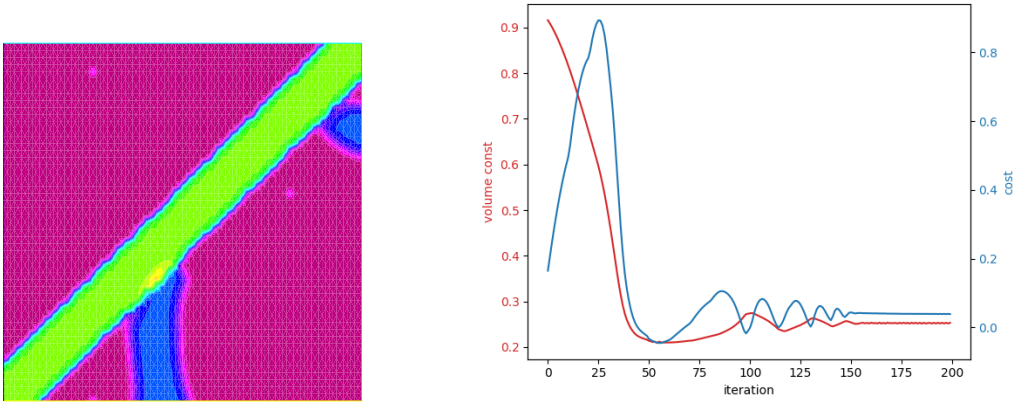

Figure 39: Anisotropic case: $E_1 = 0.1, E_2 = 1.0$

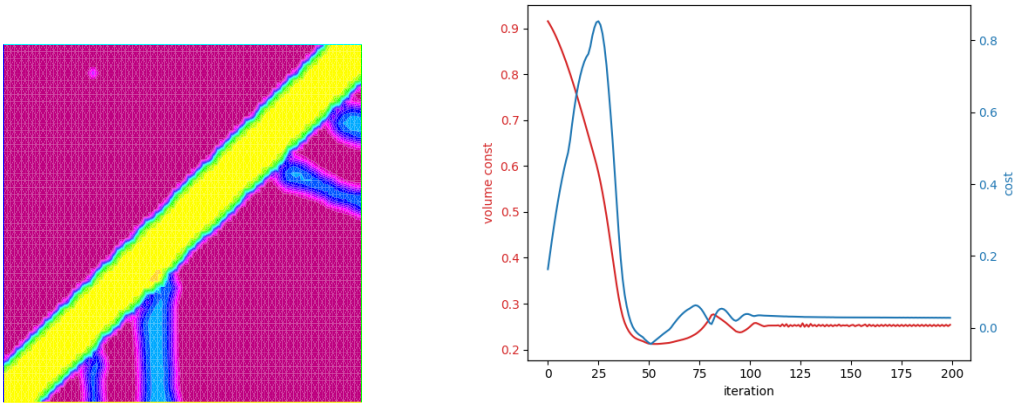

Figure 40: Isotropic case: $E_1 = E_2 = 1.0$

Remark: in the following three cases we have $V_{obj} = 1.5 \cdot V_{fixed}$.

- Case 7:

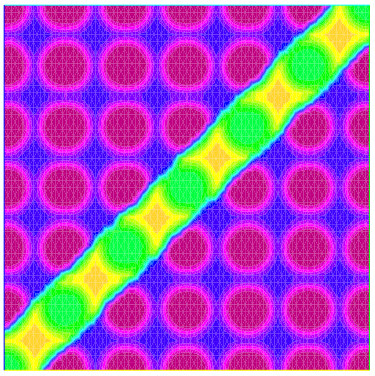

Figure 41: Initial level set function

For this configuration, we obtain the following final distribution of supports and convergence curves (volume and cost functional):

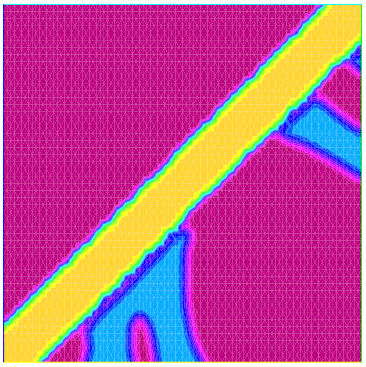

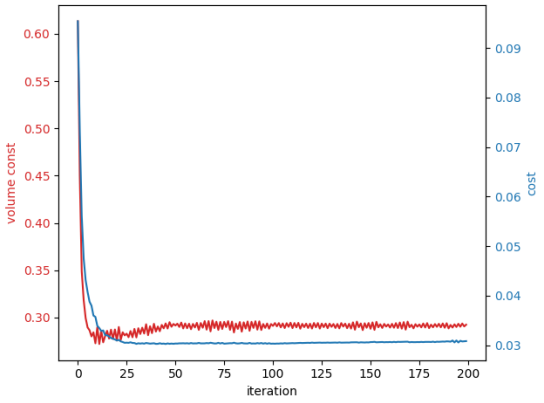

Figure 42: Anisotropic case: $E_1 = 1.0, E_2 = 0.1$

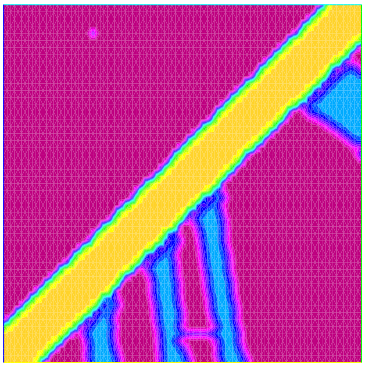

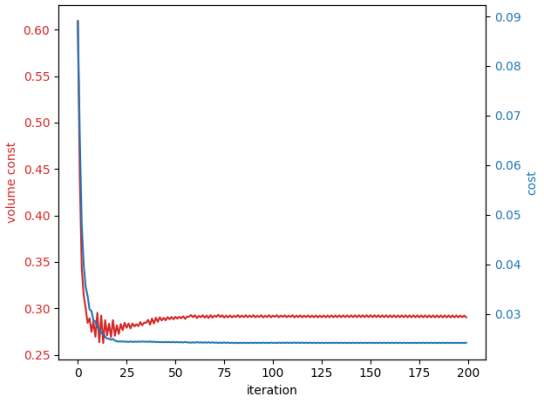

Figure 43: Anisotropic case: $E_1 = 0.1, E_2 = 1.0$

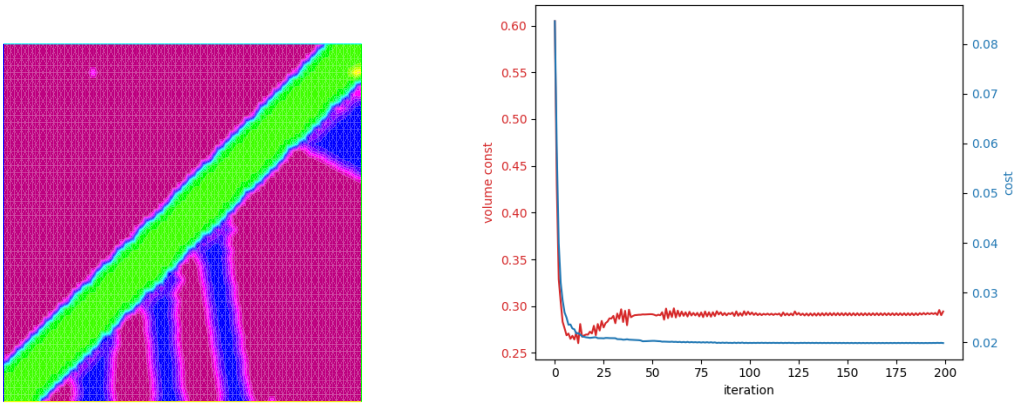

Figure 44: Isotropic case: $E_1 = E_2 = 1.0$

- Case 8:

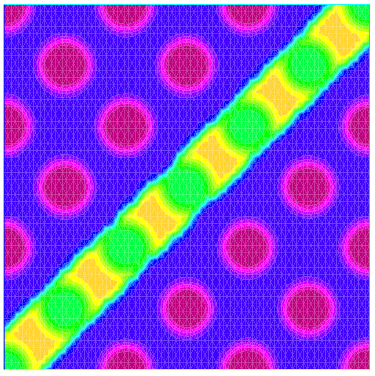

Figure 45: Initial level set function

For this configuration, we obtain the following final distribution of supports and convergence curves (volume and cost functional):

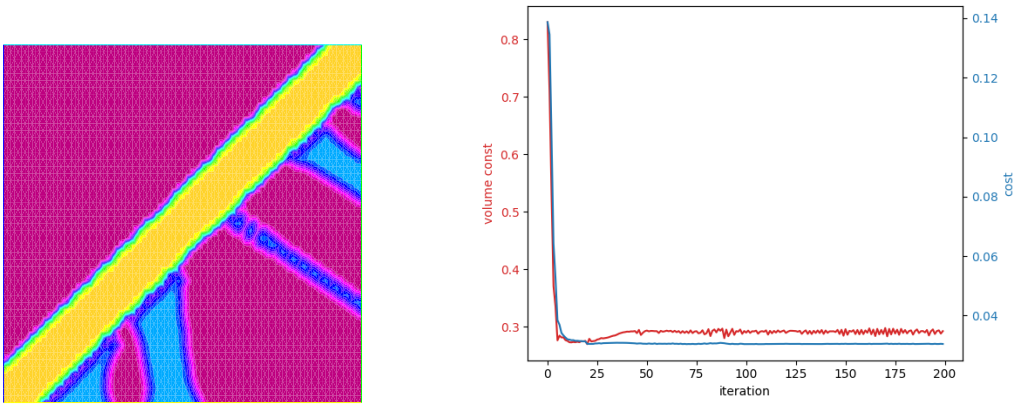

Figure 46: Anisotropic case: $E_1 = 1.0, E_2 = 0.1$

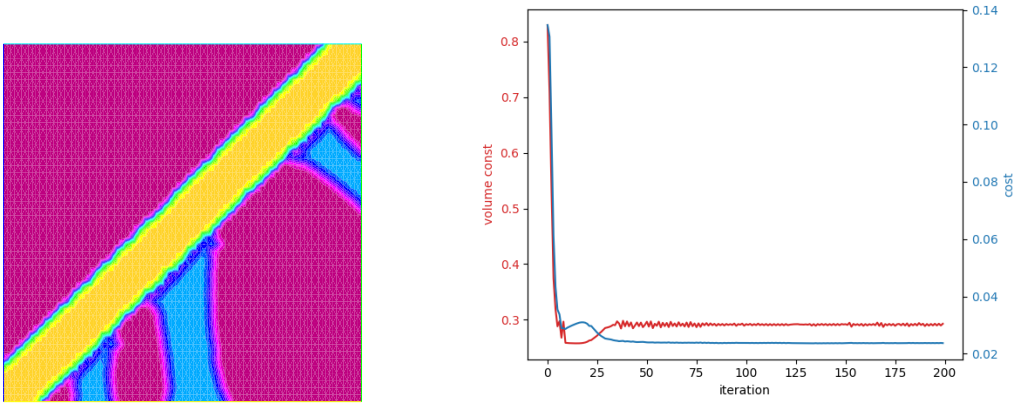

Figure 47: Anisotropic case: $E_1 = 0.1, E_2 = 1.0$

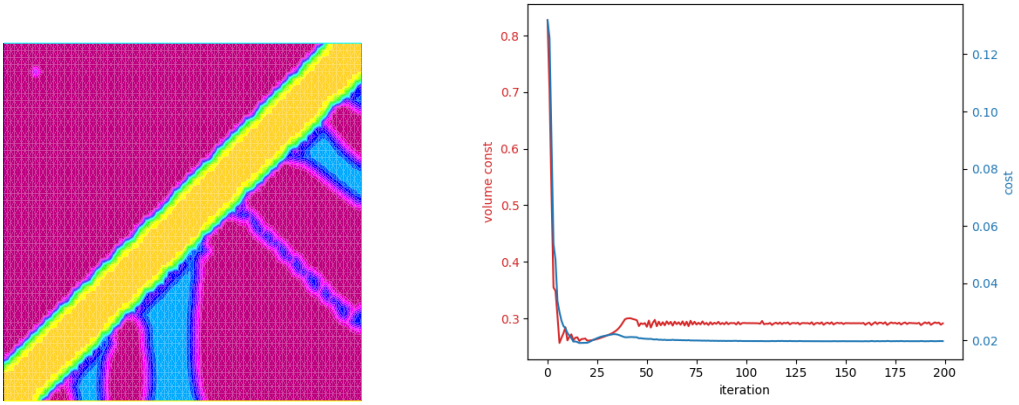

Figure 48: Isotropic case: $E_1 = E_2 = 1.0$

- Case 9:

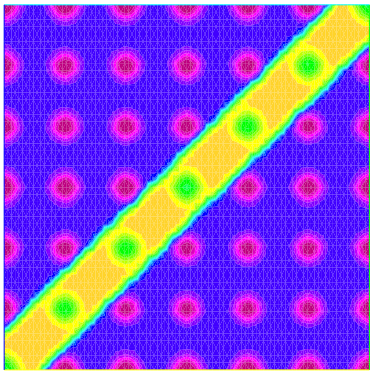

Figure 49: Initial level set function

For this configuration, we obtain the following final distribution of supports and convergence curves (volume and cost functional):

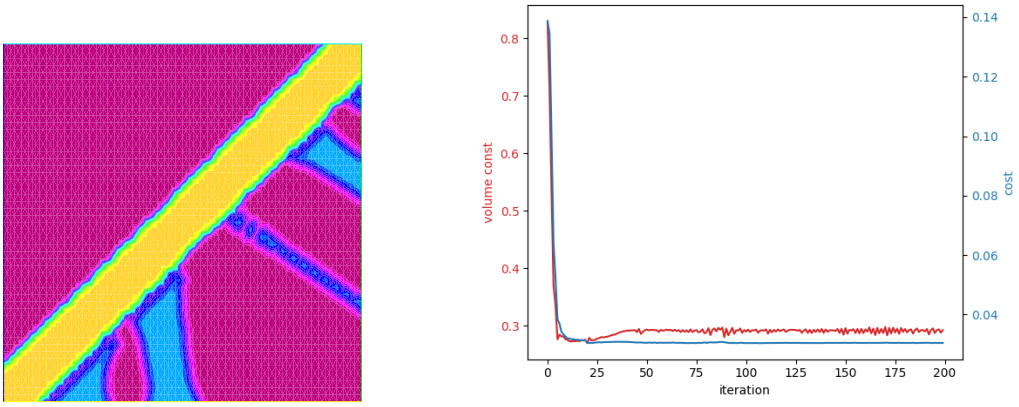

Figure 50: Anisotropic case: $E_1 = 1.0, E_2 = 0.1$

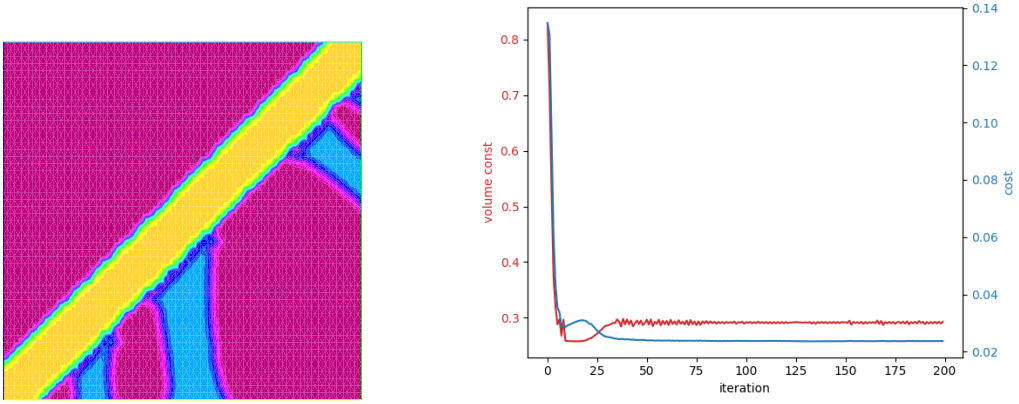

Figure 51: Anisotropic case: $E_1 = 0.1, E_2 = 1.0$

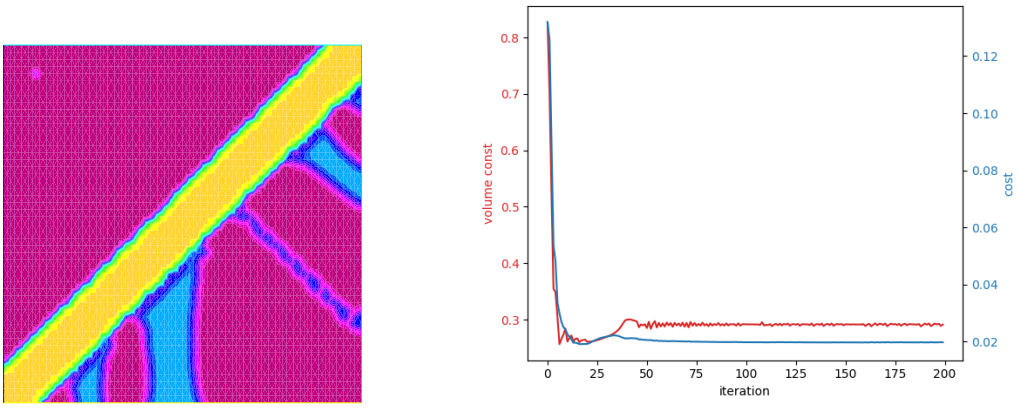

Figure 52: Isotropic case: $E_1 = E_2 = 1.0$

From these cases, we notice:

- As before, the best performance is obtained in isotropic cases.
- As expected, a higher target volume implies better performance.

- We obtain a wider variety of final configurations, with different numbers of connected components in all cases. However, qualitatively there are no remarkable differences.

3 Conclusions

From the tests performed, we can conclude:

- For the considered problem, the best performance is obtained with an isotropic configuration of the mechanical properties for the supports. Between horizontally or vertically stronger configurations, vertically stronger ones perform better in all the considered tests. However, in general, the obtained configurations are not significantly different from the isotropic case.
- The zones to be supported seem to be independent of the initial topology and of the mechanical properties of the support.
- As expected, the more material we allow for the supports, the better performance we obtain.

Finally, we believe that more general models of anisotropy should be considered in order to study the possibilities of improving the performance of the supports. Orthotropy is a particular case of anisotropy, and considering only the vertical and horizontal axes as the axes of orthotropy is a significant restriction.

Acknowledgements

The author wish to thank professors G. Allaire and B. Bogosel for their supervision and guidance in the development of this manuscript.
This work was partially supported by the SOFIA project, funded by BPI (Banque Publique d'Investissement).

References

[1] Allaire, G. and Bogosel, B. Optimizing supports for additive manufacturing. *Struct. Multidiscip. Optim.* (2018) **58(6)**:2493–2515.

[2] Allaire, G., Jouve, F., and Toader, A. M. A level-set method for shape optimization. *Comptes Rendus Mathematique* (2002), **334(12)**, 1125-1130.

[3] Allaire, G. Shape optimization by the homogenization method, *Springer Verlag, New York* (2002)

[4] Céa, J. Conception optimale ou identification de formes, calcul rapide de la dérivée directionnelle de la fonction cout. *ESAIM: Mathematical Modelling and Numerical Analysis* **20(3)** (1986): 371-402.

[5] Zienkiewicz, O.C. and Taylor, R. L. and Zhu, J.Z. The finite element method: its basis and fundamentals. *Butterworth-Heinemann.* (2005).

[6] Henrot, A. and Pierre, M. Variation et optimisation de formes: une analyse géométrique *Springer Science & Business Media.* (2006)

[7] de Gournay, F. Velocity extension for the level-set method and multiple eigenvalues in shape optimization. *SIAM J. on Control and Optim.*, **45(1)** (2006), 343–367.

[8] Hecht, F. New development in FreeFem++. *Journal of numerical mathematics* (2012) **20(3-4)** 251–266.

[9] C. Bui, C. Dapogny, and P. Frey. An accurate anisotropic adaptation method for solving the level set advection equation. *Internat. J. Numer. Methods Fluids*, **70(7)** (2012) 899–922.

[10] Osher, S., and Sethian, J. A. Fronts propagating with curvature-dependent speed: algorithms based on Hamilton-Jacobi formulations. *Journal of Computational Physics*, **79(1)** (1988), 12–49.

[11] Nocedal, J. and Wright, S. Numerical optimization. *Springer Science* (2006).